Journal of Molecular Graphics and Modelling 29 (2011) 1025–1029

Contents lists available at ScienceDirect

Journal of Molecular Graphics and Modelling

journal homepage: www.elsevier.com/locate/JMGM

Computational modeling of a rotary nanopump

A. Lohrasebi[a,b,*], Y. Jamali[c,d]

[a] Department of Physics, University of Isfahan, Isfahan, Iran
[b] Computational Physical Sciences Research Laboratory, Department of Nano-Science, Institute of Research in Fundamental Sciences (IPM), P.O. Box 19395-5531, Tehran, Iran
[c] Molecular Cell Biomechanics Laboratory, Department of Bioengineering, University of California, Berkeley, CA, United States of America
[d] Department of Physics, Amir Kabir University, Tehran, Iran

ARTICLE INFO

Article history:
Received 8 December 2010
Received in revised form 20 April 2011
Accepted 21 April 2011
Available online 5 May 2011

Keywords:
Rotary nanopump
Nanotube
Graphene blades
Molecular dynamics method
Atomic gradient
Rotor frequency

ABSTRACT

The dynamics of a rotary nanopump, consisting of three coaxial carbon nanotubes and a number of graphene blades, has been simulated via application of the molecular dynamics (MD) method. In this nanopump the inner nanotube, the middle carbon nanotube with together the graphene blades and the outer nanotube are used as the shaft, rotor, and sleeve of the pump, respectively. The rotary motion of the rotor is due to the mechanical rotation of the two first carbon rings of the rotor's carbon nanotube. We found that this pump flow the gas atoms between two sides of the nanopump and it can produce an atomic gradient. Also it is observed that a rotary frequency of the rotor affected on the pump performance for generating the density gradient and the maximum performance is occurred at a special frequency of the rotor. This special rotary frequency can be computed by an analytical formula, for given material and temperatures. Moreover, the results indicate that the number of the rotor's graphene blades do not have a significant effect on the pumping capacity. Our finding provides a potentially useful mechanism for gas purification process.

1. Introduction

The protein motors, which generate mechanical motion from chemical energy, play an important role in all life processes. These nanomotors can be divided into two main groups. The first group is the rotary nanomotor such as F_0F_1-ATP synthase [1,2] or bacterial flagella protein motor [3] that produces the rotary motion from the stored energy in the ion gradient between two sides of the motor. The second group is the linear motor such as myosin and kinesin [4] protein motors. These linear motors transport a variety of cargoes, like vesicles, in the stochastically fluctuating intracellular medium by using the chemical energy, released during the hydrolysis of the ATP (adenosine three phosphate) molecules.

Inspired by the protein motors, nano-scale motors can be proposed to use in nanotechnology. The single-walled carbon nanotubes (SWCNTs) are usually used to design nano-scale devices, such as nanomotors [5–7], nanopump [8–10], nanocarrier [11], bearings [12] and oscillators [13]. Here, we briefly review some of the conceptual nanomotors that have been designed in the past. Tuzun et al. have developed a laser-driven nanomotor [5], which is simulated by application of the molecular dynamics (MD). This nanomotor is constructed of two concentric nanotubes, acting as a sleeve and a shaft, where a pair of positive and negative electric charges was located on two carbon atoms of the end ring in the sleeve part. An oscillating electric field is used to induce a rotary motion in the sleeve. The full rotary motion is observed just at an optimum range of the field's frequency that the optimum range of the field's frequency is dependent on the size of the motor, and the relative positions of the attached charges.

Another MD simulation studied, Han et al. investigated the stability of the mechanically-driven nanogear [6]. They demonstrated that when the atoms near the end of the nanotube in one gear are enforced to rotate, the second nanotube begins to rotate as well.

In the other simulation [7], a nanoscale rotary motor driven by electron tunneling was examined. In this studied, the nanomotor is made of a carbon nanotube as a shaft with covalently attached isolating molecular stalks ending with conducting blades. Periodic charging and discharging of the blades at two metallic electrodes maintains an electric dipole on the blades that was rotated by an external electric field.

A further MD-based simulation has designed a nanopump [10] by using single-walled carbon nanotube (SWNT) to pumping molecules along the SWNT axis, via mechanical wave propagation driven by an oscillating tip actuator.

Recently, another MD-based simulation studied [14], a nanopropeller formed from a functionalised (8,0) SWCNT. The propeller pumped liquid due to an imposed rotation on its blades. The blades were made from pyrene molecules and attached to the opposite

* Corresponding author at: Department of Physics, University of Isfahan, Isfahan, Iran. Tel.: +98 3117934842; fax: +98 2122835058.
E-mail address: lohrasebi@phys.ui.ac.ir (A. Lohrasebi).

1093-3263/$ – see front matter © 2011 Elsevier Inc. All rights reserved.
doi:10.1016/j.jmgm.2011.04.007

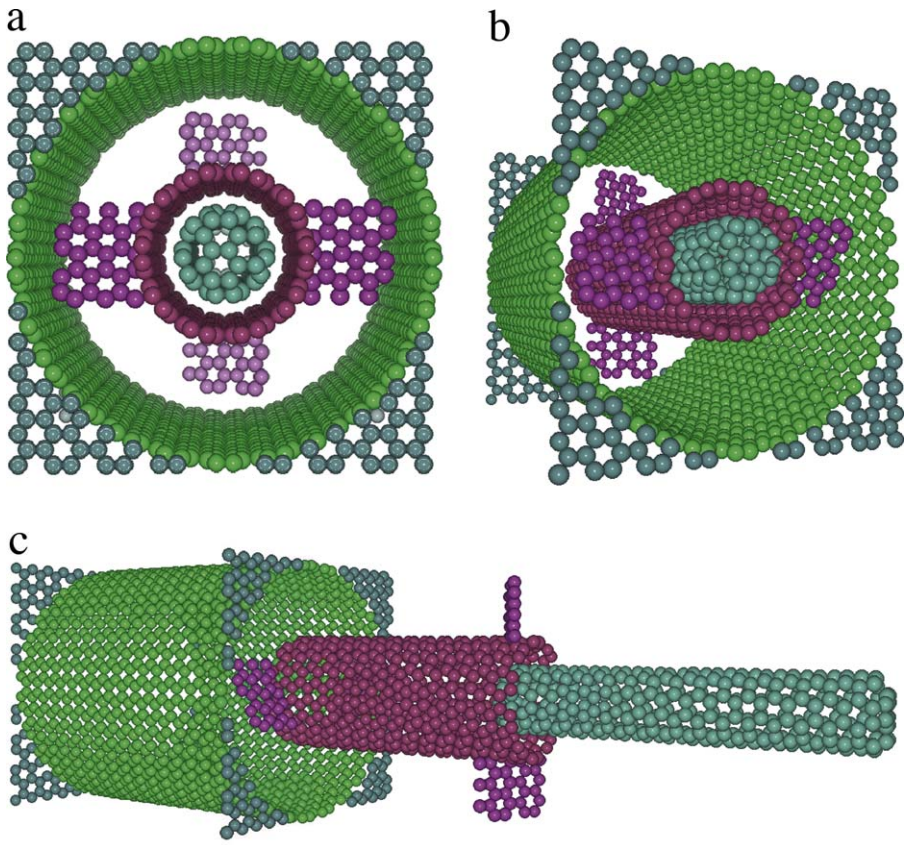

Fig. 1. The structure of the nanopump components: (a) front view of the rotor. The rotor is composed of a nanotube and four graphene blades attached to the opposite sides of the rotor at distal ends of the rotor axis and tilted with respect to its axis; (b) three dimensional view of of the nanopump; (c) the complete structure of the nanopump that shown separately.

sides of the nanotube and were tilted with respect to its axis. The simulation revealed that pumping depended significantly on the chemistry of the blade–liquid interface and also to the size, shape, chemical, or biological compositions of the nanoblades.

In our previous work [15], we proposed a nano-scale ion-driven rotary motor inspired by the F_0 part of ATPase protein-motor. That motor was constructed from SWCNTs, benzene rings and graphene sheets. The dynamics of that nanomotor in the presence and absence, of an external electric field has been simulated via stochastic molecular dynamics. The rotary motion of the proposed motor was resulted from an ion gradient established between the outer and inner parts of the environment containing the motor.

In this paper, we have proposed a nano-scale pump constructed of SWCNTs and graphene blades. The classical MD simulation [16] has been employed to simulate the dynamics of this rotary nanopump.

2. Atomistic structure of the proposed nanopump

The schematic structure of the proposed nanopump is shown in Fig. 1. Our proposed nanopump is composed of three sections. The first section is the shaft, which is made of a (5,5) capped nanotube with a length of 40 Å and a radius of 3.443 Å. The second section of the nanopump, named *rotor*, is made of a (10,10) nanotube with the same shaft length and a radius of 6.9 Å. As shown in Fig. 1(a) and (c), two pairs of graphene blades with the same area equal to 8.4×6 Å^2, are attached to the two ends of the rotor and tilted with respect to the rotor's axis. The third section of the nanopump is made of a (25,25) nanotube with a radius of 17.33 Å and is named the *pump sleeve*, which surrounds the rotor. Two identical boxes connect to the sides of the pump, one initially empty and the other filled with gas atoms. Since the boxes are cubic and the pump is cylindrical, two square graphene sheets are added to the pump to force the gas atoms to pass only through the pump to travel between boxes. These square graphene sheets have a central hole with a radius of 18.7 Å and are attached to the two ends of the pump sleeve.

3. Computational details

Our system has 1250 gas atoms. The number of carbon atoms in the nanopump is 2967, 3021 and 3075 for the rotor with two, four and six blades, respectively. The particles are confined in a rectangular box with dimensions of $L_x = 300$, $L_y = 37$ and $L_z = 37$ Å. Periodic boundary conditions are applied in the y- and z-directions and the temperatures is varied between 50 and 1100 K.

Two types of interatomic potential are used in our simulations. The first generation of Brenner potential [17] is used for modeling the covalent bonding between the carbon (C) atoms within the nanotubes and within the graphene blades. The Lennard–Jones (LJ) potential is used to describe the non-bonding interactions between the gas atoms and the carbon atoms as well as for carbon–carbon interactions between the different parts of the nanopump. The parameters of the LJ potential are $\epsilon_{Ne} = 0.003121$ eV, $\sigma_{Ne} = 2.75$ Å or $\epsilon_{He} = 0.000867$ eV, and $\sigma_{He} = 2.55$ Å [18], for the gas atoms, and $\epsilon_C = 0.002413$ eV and $\sigma_C = 3.4$ Å for the C–C interaction [18]. The parameters for the gas atoms and carbon atoms interaction are calculated by using the Lorentz–Berthelot mixing rules, i.e., $\epsilon_{\text{gas}-C} = \sqrt{\epsilon_{\text{gas}} \times \epsilon_C}$, and $\sigma_{\text{gas}-C} = 0.5(\sigma_{\text{gas}} + \sigma_C)$.

The dynamics of all atoms are described by Newton's differential equation and velocity Verlet method [16] is used for time integration, with a time-step of 0.5 fs. The simulations are

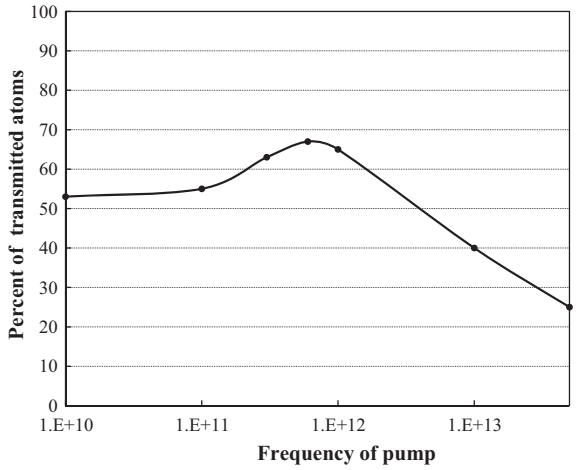

Fig. 2. The percent of Neon atoms that pass through the pump, as a function of the pump frequency at $T = 300$ K.

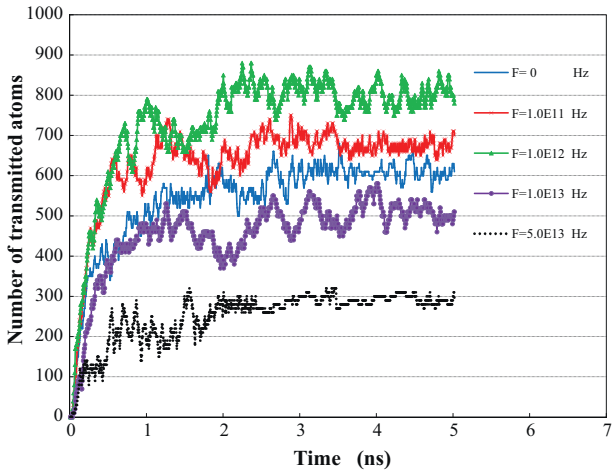

Fig. 3. The net number of the Neon atoms that pass through the pump as a function of the simulation time, for several rotor frequency at $T = 300$ K.

performed via our custom-written FORTRAN MD code, considers a constant-*NVT* ensemble. The temperature control is implemented with the Nosé-Hoover thermostat scheme [19,20] for the velocity Verlet algorithm [21].

4. Results and discussion

The nanopump is equilibrated for 250 ps at constant temperatures in the absence of the gas atoms. Then we forced the two tip rows of the carbon atoms in the rotor to rotate and hence induced a rotary motion for the whole rotor. At this time, the gas atoms entered the box. The temperature is fixed and the rotor speed is varied between different simulations.

It is observed that, the gas atoms travel from the full box to the other box. The rotation of the pump causes an density gradient between its entries. For example, for the Neon atoms as the gas atoms, at the temperature of 300 K and at the low frequency (below 10^{11} Hz), the transport rate is increased slightly with the increase of the rotor frequency. Then in the rotor frequency range of $10^{11} - 10^{12}$ Hz it reaches to a maximum value, and for the higher frequencies (above 10^{12} Hz) this rate is reduced. Fig. 2 shows this behavior for the Neon atom at $T = 300$ K. It seems that, above the frequency range of 5×10^{13} Hz, rotation of the rotor obstructs the pump. Indeed once gas atom is placed near the entrance of the pump, r_0, it senses the blades atoms due to the non-bonding interaction. This distance, i.e. r_0, is defined as to be in the range of the equilibrium distance between two atoms and its value can be found by differentiating the non-bonding interatomic potential (this value in the LJ potential is equal 1.122σ, where σ is the specific length of the LJ potential). To be more specific, a gas atom can only enter to the pump provided that it does not face the rotating blades in the entrance of the pump. This condition can be satisfied if the interval time t, for a gas atom to enter to the pump, is less than the half of the periodic time of the rotor (if the rotor has three blades, the interval time must be less than one third of the periodic time). Since the interval time, t, is dependent on the velocity of the gas atoms, and hence related to the gas temperature; we propose a relation between optimum frequency and gas temperature:

$$t = \frac{r_0}{v_x} \quad v_x = \sqrt{\frac{k_B T}{m}} \text{ and } t \simeq \frac{1}{2f} \Rightarrow f \simeq \sqrt{\frac{k_B T}{4 m r_0^2}} \tag{1}$$

Here r_0 corresponds to the distance between the gas atom and carbon atom of the blade, v_x is the x component of the gas atom velocity, k_B correspond to the Boltzmann constant, T is the temperature, m is the atomic mass of the gas atom and finally f refers to the rotor frequency. For example for the Neon and the Helium atoms, at 300 K temperature, the optimum frequencies are predicted to be around 0.6×10^{12} Hz and 1.4×10^{12} Hz, respectively. So if we have mixture of the Neon and the Helium gas atoms at $T = 300$ K and the rotor frequency is equal to 0.6×10^{12}, which is the optimum frequencies of the Neon atom, the transferring rate of the Neon atoms will be more than the Helium atoms. Hence this pump can be used to separate the mixture of gas atoms.

At $T = 300^\circ$ K and in the frequency range of 5×10^{13} Hz, the half of the period of the rotor rotation is much smaller than the interval time of the gas atoms (compare $t = 1.7 \times 10^{-12}$ s for the Neon atoms, with 1×10^{-14} s, which is the half of the period of the rotor rotation). Hence when a gas atom is closing to the entrance of the pump, this entrance looks blocked to it by blades for most of the time. Hence, the repulsive force between the gas atom and blade atoms pushes it away from the pump entrance and consequently the transport rate is reduced.

Fig. 2 shows the percent of Neon atoms that pass through the pump, as a function of the pump frequency (the percent of transmitted atoms is equal to the number of atoms that passed trough the pump over the total number of gas atoms). This curve's maximum is reached at a frequency range between 0.6×10^{12} and 0.7×10^{12} Hz at $T = 300$ K, which is harmony with the obtained result from Eq. 1. Fig. 3 shows the net number of the Neon atoms that pass through the pump as a function of the simulation time at a temperature of $T = 300$ K. This figure covers several rotor frequencies. It can be observed that at initial times, the net number of the transmitted atoms increases and then it fluctuates around a fixed value. By

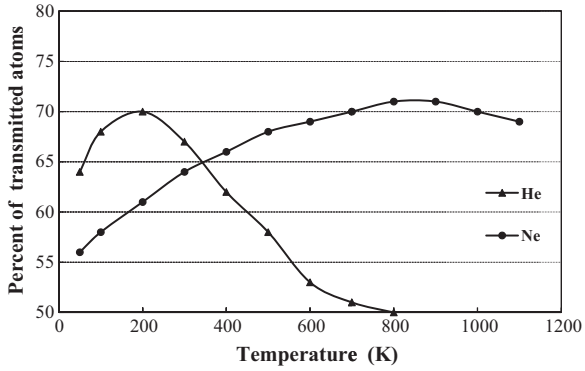

Fig. 4. The percent of transmitted atoms versus temperature for the gas atoms (Ne and He) at the rotor frequency of 10^{12} Hz.

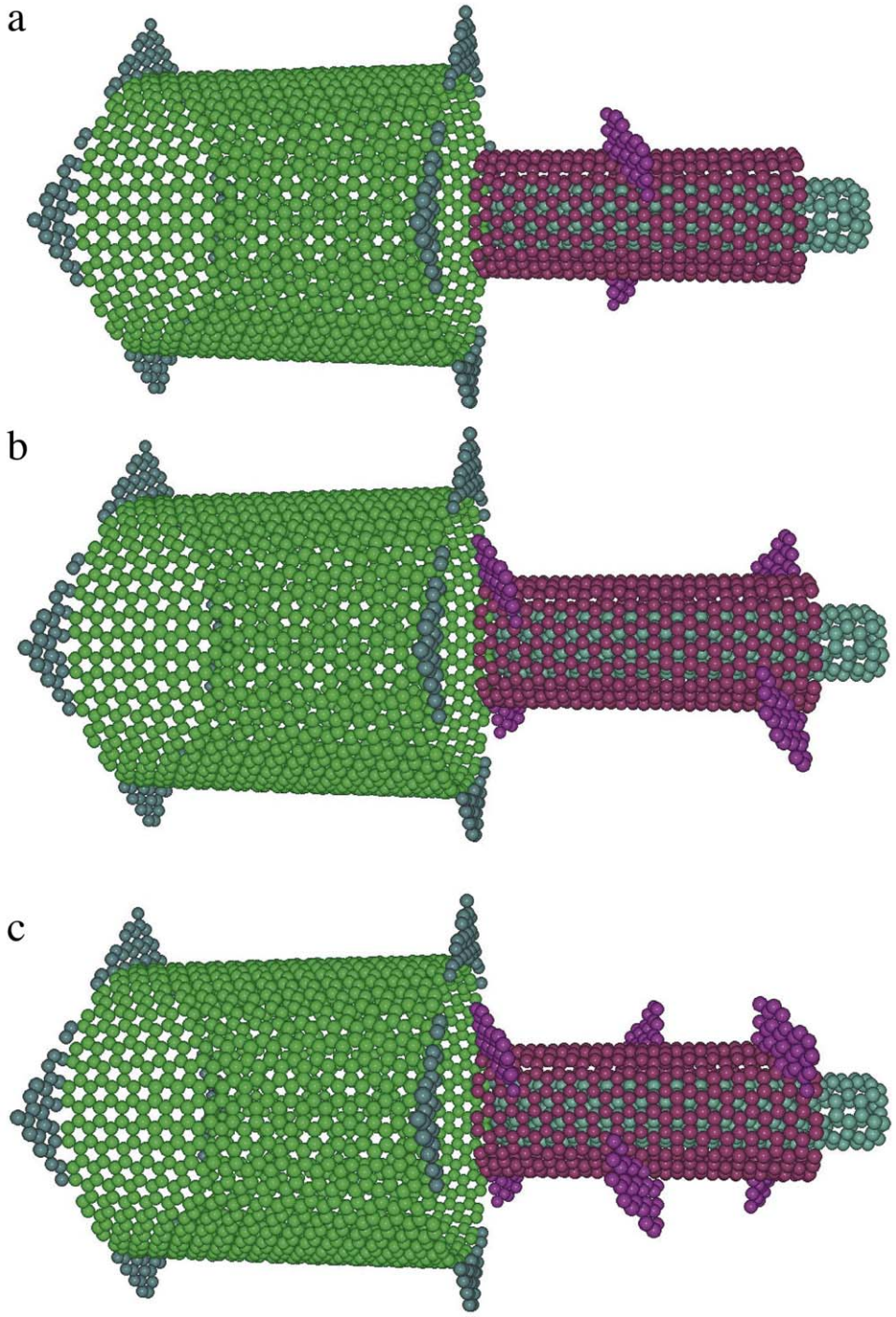

Fig. 5. Complete structure of the nanopump that shown separately: (a) two-blades rotor; (b) four-blades rotor; and (c) six-blades rotor.

comparing this curves between the non zero frequency and zero frequency, it is observed that when the rotor rotates, it enhances the transport rate of the gas atoms. Hence as demonstrated in Fig. 2, the pump has an ability to create an density gradient between the two boxes. The amount of this density gradient is dependent on the rotor frequency. For example the density gradient that is produced for $f = 10^{11}$ Hz is not equal to the density gradient in $f = 10^{12}$. Also, according to Fig. 3, when the rotor frequency is in the range of the optimum frequency, the gas atoms pass through the pump faster than stationary pump (zero frequency). Hence, this pump can be used as a device to control the rate of atoms transport or to produce a gradient between two containers.

Fig. 4 shows the effect of temperature on the ability of nanopump to produce the density gradient (we named it the pump capacity), for Ne and He atoms, at a frequency of 10^{12} Hz. It can be observed that for the Helium atoms, the percent of transmitted atoms through the pump (PTATP), reached to its maximum value at $T = 200$ K, but this value for the Neon atoms is found at $T = 900$ K. By using Eq. (1) to calculate the temperature in which the optimum frequency of the rotor is equal to 10^{12} Hz, we will find $T = 175$ K and $T = 870$ K for Helium and Neon atoms, respectively. The predicted values, by Eq. (1) are close to the values that can be found from Fig. 4. In fact the PTATP for Ne and He atoms, at the same temperature and the rotor frequency, are different because of

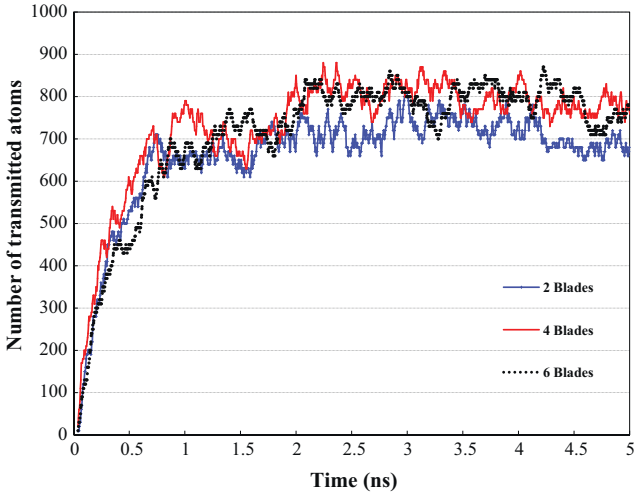

Fig. 6. The net number of the transmitted Neon atoms versus blade number of the rotor at $T = 300$ K and the rotor frequency of 10^{12} Hz.

difference in the mass of Ne and He atoms. For example at $T = 200$ K and $f = 10^{12}$ Hz the PTATP for Ne atoms is equal to 61 percent and for He atoms is equal to 70 percent, as can be seen in Fig. 4. So the pump can extract and purify helium from the mixture of these two gases at 200 K and the pump frequency of $f = 10^{12}$ Hz. Also it can be seen from Fig. 4 that for the other temperatures, the ability of the pump to produce the density gradient will be reduced (like He gas at the $T \neq 200$ K and $f = 10^{12}$ Hz).

To evaluate the influence of the number of rotor blades on the pump capacity, we used the rotor by two, four and six blades for pumping the gas atoms. The structures of these three nanopumps are shown in Fig. 5. Fig. 6 shows the effect of number of rotor blades on the pumping for the Neon atoms at $T = 300$ K and the rotor frequency of 10^{12} Hz. As can be observed, the number of rotor's blades does not have a significant effect on the pump capacity.

5. Conclusions

In this work, we have provided the outline of a nano-scale pump. Deterministic MD simulations, based on many-body, and two-body, interatomic potentials, are employed to model the dynamics of a nanopump. We investigated the influence of parameters, such as temperature or number of blades on the operation of the pump. It is found that this pump can produce density gradient along its axis and for each temperature, there is an optimal frequency that results in the largest amount of atomic gradient. We have also proposed an analytical solution to find the optimal frequency of the rotor for different gass as a function of the temperature. Furthermore, our simulations reveal that the number of the blades does not have a significant effect in the pump capacity. Also this pump can be used in gas extraction/ purification process. The productivity of the pump is related to the difference of molecular mass of mixture elements.

Acknowledgment

We gratefully acknowledge Reza Karimi for his valuable comments on the manuscript.

References

[1] J. Xing, H. Wang, C.V. Ballmoos, P. Dimroth, G. Oster, Torque generation by the F0motor of the sodium ATPase, Biophys. J. 87 (2004) 2148–2163.
[2] A. Lohrasebi, Y. Jamali, H. Rafii-Tabar, Modeling the effect of external electric field and current on the stochastic dynamics of ATPase nano-biomolecular motors, Physica A 387 (2008) 5466–5476.
[3] D.J. DeRosier, The turn of the screw: the bacterial flagellar motor, Cell 93 (1998) 17–20.
[4] Y. Jamali, A. Lohrasebi, H. Rafii-Tabar, Computational modeling of the stochastic dynamics of kinesin biomolecular motors, Physica A 381 (2007) 239–254.
[5] R.E. Tuzun, D.W. Noid, B.G. Sumpter, Dynamics of a laser driven molecular motor, Nanotechnology 6 (1995) 52–63.
[6] J. Han, A. Globus, R. Jaffe, G. Deardorff, Molecular dynamics simulation of carbon nanotube-based gears, Nanotechnology 8 (1997) 95–102.
[7] B. Wang, L. Vukovic, P. Kral, Nanoscale rotary motors driven by electron tunneling, Phys. Rev. Lett. 101 (2008) 1868081–1868084.
[8] X. Gong, J. Li, H. Lu, R. Wan, J. Li, J. Hu, H. Fang, A charge-driven molecular water pump, Nature 2 (2007) 709–712.
[9] Z. Insepov, D. Wolf, A. Hassanein, Nanopumping using carbon nanotubes, Nano Lett. 6 (2006) 1893–1895.
[10] M. Chen, J. Zang, D. Xiao, C. Zhang, F. Liu, Nanopumping molecules via a carbon nanotube, Nano Res. 2 (2009) 938–944.
[11] A. Barreiro, R. Rurali, E.R. Hernández, J. Moser, T. Pichler, L. Forró, A. Bachtold, Subnanometer motion of cargoes driven by thermal gradients along carbon nanotubes, Science 320 (2008) 775–778.
[12] S. Zhang, W.K. Liu, R.S. Ruoff, Atomistic simulations of double-walled carbon nanotubes as rotational bearings, Nano Lett. 4 (2004) 293–297.
[13] J.W. Kang, K.O. Song, O.K. Kwon, H.J. Hwang, Carbon nanotube oscillator operated by thermal expansion of encapsulated gases, Nanotechnology 16 (2005) 2670–2676.
[14] B. Wang, P. Kral, Chemically tunable nanoscale propellers of liquids, Phys. Rev. Lett. 98 (2007) 266102 1–2661024 2661024.
[15] A. Lohrasebi, H. Rafii-Tabar, Computational modeling of an ion-driven nanomotor, J. Mol. Graph. Model. 27 (2008) 116–123.
[16] M.P. Allen, D.J. Tildesley, Computer Simulation of Liquids, Clarendon, Oxford, 1987.
[17] D.W. Brenner, Phys. Empirical potential for hydrocarbons for use in simulating the chemical vapor deposition of diamond films, Phys. Rev. B 42 (1990) 1–14, 9458.
[18] G. Stan, M.J. Bojan, S. Curtarolo, S.M. Gatica, M.W. Cole, Uptake of gases in bundles of carbon nanotubes, Phys. Rev. B 62 (2000) 2173–2180.
[19] S. Nosé, A unified formulation of the constant temperature molecular dynamics method, J. Chem. Phys. 81 (1984) 511–519.
[20] W.G. Hoover, Canonical dynamics: equilibrium phase-space distributions, Phys. Rev. A 31 (1985) 1695–1697.
[21] H. Rafii-Tabar, Modelling the nano-scale phenomena in condensed matter physics via computer-based numerical simulations., Phys. Rep. 325 (2000) 239–310.